A Combined Barotropic–Baroclinic Instability Study of the Upper Tropospheric Tropical Easterly Jet

S. K. MISHRA AND M. K. TANDON

Indian Institute of Tropical Meteorology, Pune-411 005, India

(Manuscript received 11 January 1983, in final form 23 June 1983)

ABSTRACT

A combined barotropic–baroclinic stability analysis is performed for an upper tropospheric tropical easterly jet representing the observed mean monsoon zonal flow during summer. Numerical solutions are obtained by time integration of a 20-layer linear spectral quasi-geostrophic model, which is based on truncated Fourier series representations in y. It is seen from the growth rate and phase speed spectra that the asymmetric barotropic–baroclinic preferred wave has a wavelength of 6500 km, an e-folding time of 3.3 days, a westward phase speed of 20.5 m s^{-1} and a period of 3.8 days.

The geopotential, vertical velocity and temperature fields associated with the most unstable barotropic–baroclinic wave are computed. The most unstable wave has a vertical scale of 125 mb, a meridional scale of 1650 km and a zonal scale of 2135 km. The relationship between the vertical and meridional scales of the wave with the corresponding basic zonal flow scales is discussed.

The large southward easterly momentum transports associated with the unstable wave are essentially due to the antisymmetric components of the jet. The computed sensible heat transports are found to be down the basic state meridional temperature gradient. The energetics of the unstable wave is computed and it is inferred that the energy sources for the wave growth lie in a narrow vertical layer around the jet level. It is also found that the contribution of baroclinic process is larger than the contribution of barotropic processes in the wave growth.

The contributions of different physical processes in the movement of the unstable wave are also investigated. The beta effect is identified as the most important physical factor responsible for the westward propagation of the wave.

1. Introduction

An observational study of Krishnamurti (1971) based on wind data at 200 mb surface during a northern summer has indicated that the synoptic-scale transient disturbances, in the vicinity of the tropical upper tropospheric easterly jet, have a zonal wavelength in the range of 5000–7000 km, a westward phase speed of 10–12° longitude day^{-1} and the preferred latitude for the development of these waves is to the south of the jet core. These observed characteristics of the waves are supported by a nondivergent barotropic simulation experiment of stationary planetary waves (wavenumbers 1–3) at 200 mb during the northern summer (Colton, 1973).

It has been shown that the baroclinic instability of the easterly jet can lead to the formation and the initial growth of waves of wavelength around 6000 km (Mishra and Salvekar, 1980; Salvekar and Mishra, 1984). A barotropic stability analysis of the observed mean asymmetric easterly jet at 100 mb was performed by Mishra *et al.* (1981) who found that many features of the most unstable mode, such as the associated momentum transports, the latitude of wave amplitude maximum and the wave meridional scale, are in reasonable agreement with observations.

The purpose of this study is to investigate the characteristics of the most unstable mode of the easterly jet with meridional and vertical shears, in order to provide a qualitative basis for understanding the initial development and movement of the upper tropospheric disturbances. Shukla (1977) performed a barotropic–baroclinic stability analysis of the July mean zonal wind distribution along longitude 85°E. He obtained a preferred wave of wavelength 3000 km whose amplitude maximum is located to the far north of the easterly jet core—a value not in as good agreement with the observed values as mentioned above.

2. System of equations

a. The linear quasi-geostrophic model and boundary conditions

We assume the atmospheric motions are adiabatic, inviscid and in hydrostatic equilibrium. The Rossby radius of deformation (2000 km), the average vertical half-width of the easterly jet (150 mb; Mokashi, 1974) and the wind velocity (10 m s^{-1}) have the characteristic horizontal length, pressure and horizontal velocity scales associated with the upper tropospheric disturbances along the easterly jet. The average static stability

in the easterly jet region is ~ 0.17 m^2 s^{-2} mb^{-2}. Scale analysis shows that the upper tropospheric wave motions around the latitude (15°N) of the jet's center are quasi-geostrophic to a first order of approximation. Krishnamurti (1971) has further shown that synoptic-scale motions at 200 mb are predominately rotational even in the equatorial latitudes. It is probable that solutions obtained in this study are distorted near the equator due to non-inclusion of ageostrophic effects and the complete latitudinal variation of the Coriolis parameter in this study. The lower tropospheric wave motions have been presented in several earlier works utilizing quasi-geostrophic models (Mak, 1975; Estoque and Lin, 1977; Mak and Kao, 1979; and others).

The linear quasi-geostrophic vorticity and thermodynamic equations for an infinitesimal perturbation superimposed on a basic state zonal flow $\bar{u}(y, p)$ can be written as

$$\nabla^2\phi_t + \bar{u}\nabla^2\phi_x + (\beta - \bar{u}_{yy})\phi_x - f_0^2\omega_p = 0, \quad (1)$$

$$\phi_{pt} + \bar{u}\phi_{px} - \bar{u}_p\phi_x + \sigma\omega = 0, \quad (2)$$

where ϕ and ω are the perturbation geopotential and vertical velocity, respectively, $\bar{u}(y, p)$ is the basic state geostrophic wind, f_0 and β are the Coriolis and Rossby parameters, respectively, and σ is the static stability which is a function of p alone. In the above equations, the coordinate variables as subscripts denote differentiation with respect to the respective variables.

The quasi-geostrophic omega equation is obtained by eliminating time tendency terms between Eqs. (1) and (2), giving

$$\sigma\nabla^2\omega + f_0^2\omega_{pp} = [(\bar{u}\nabla^2 + \beta - \bar{u}_{yy})\phi_x]_p - \nabla^2(\bar{u}\phi_{xp} - \bar{u}_p\phi_x). \quad (3)$$

The first and second terms on the right hand side of Eq. (3) represent the effect of differential absolute vorticity advection and the Laplacian of thermal advection, respectively. The quasi-geostrophic omega represents the vertical motion associated with the large-scale systems that is needed to maintain the geostrophic and hydrostatic balances.

We have assumed rigid horizontal surfaces at the top and bottom of the atmosphere. This implies the following vertical boundary conditions:

$$\omega = 0 \quad \text{at} \quad p = 0 \quad \text{and} \quad p = p_0, \quad (4)$$

where p_0 is the constant surface pressure.

We solve the equations for a channel of the atmosphere bounded by the rigid vertical walls at $y = 0$ and $y = D$, where D is the channel width. The lateral boundary conditions in terms of the geopotential field are

$$\phi = 0 \quad \text{at} \quad y = 0 \quad \text{and} \quad y = D. \quad (5)$$

As has been shown by Phillips (1954), the following additional boundary conditions are required to ensure the conservation of energy and to obtain a unique solution for an atmospheric motion in a channel:

$$\int_0^{2\pi/k} \phi_{yt}dx = 0 \quad \text{at} \quad y = 0 \quad \text{and} \quad y = D, \quad (6)$$

where k is the zonal wavenumber. Harmonic wave solutions automatically satisfy these additional boundary conditions, because the zonally averaged ϕ is zero throughout the channel, including the lateral boundaries.

b. Energy equations

The area-averaged perturbation energy equations are obtained from Eqs. (1) and (2). We define the area-averaged wave kinetic energy $\{K_w\}$, the wave available potential energy $\{P_w\}$, the basic state kinetic energy $\{K_b\}$, and the available potential energy $\{P_b\}$ over the area $0 \leq x \leq L$ (zonal wavelength), $0 \leq y \leq D$ as

$$\{K_w\} = \{\overline{\nabla\phi \cdot \nabla\phi}\}/(2f_0^2), \quad (7a)$$

$$\{P_w\} = \{\overline{\phi_p^2}\}/(2\sigma), \quad (7b)$$

$$\{K_b\} = \{\bar{u}^2\}/2, \quad (7c)$$

$$\{P_b\} = \{\bar{\phi}_p^2\}/(2\sigma), \quad (7d)$$

where the bars denote the zonal average and the braces the area average.

The area-averaged wave kinetic energy equation can be written as

$$\{K_w\}_t = C\{K_b, K_w\} + C\{P_w, K_w\} + VK_wC, \quad (8)$$

where $C\{K_b, K_w\}$ denotes the barotropic energy conversion, $C\{P_w, K_w\}$ denotes the baroclinic energy conversion from the wave available potential energy to the wave kinetic energy, and VK_wC stands for the vertical wave kinetic energy flux convergence. The energy conversions and the wave energy flux convergence appearing in Eq. (8) are defined as

$$C\{K_b, K_w\} = -\{\bar{u}(\overline{\phi_x\phi_y})_y\}/f_0^2, \quad (9a)$$

$$C\{P_b, K_w\} = \{\overline{\phi_p\omega}\}, \quad (9b)$$

$$VK_wC = -\{(\overline{\phi\omega})_p\}. \quad (9c)$$

The time rate of change of the area-averaged available potential energy equation can be written as

$$\{P_w\}_t = C\{P_b, P_w\} - C\{P_w, K_w\}, \quad (10)$$

where $C\{P_b, P_w\}$ denotes the energy conversion from the basic state available potential energy to the wave available potential energy, which is given by

$$C\{P_b, P_w\} = \{\bar{u}_p(\overline{\phi_x\phi_p})\}/\sigma. \quad (11)$$

c. Necessary condition for instability

It is always desirable to see whether or not the zonal wind distribution satisfies the necessary condition for

the instability before performing a detailed stability analysis of the flow, in order to avoid unnecessary computations and minimize the possibility of obtaining unphysical unstable modes. The necessary condition requires that the meridional gradient of the basic state potential vorticity $\bar{q}_y$ $[=\beta - \bar{u}_{yy} - (\bar{u}_p/\sigma)_p]$ should vanish at some point in the meridional plane and change sign around this point. In other words, $\bar{q}_y$ should have at least a proper local extremum in the region.

Brown (1969) has pointed out that the major advantage of the initial value approach is that it requires less computer storage per degree of freedom than the eigenvalue approach. The principal disadvantage of this approach is that it provides solutions corresponding to only the fastest growing modes. Since the primary objective of our study is to explain the initiation and intensification of the upper tropospheric monsoon disturbances, the fastest growing modes are considered to be sufficient for this purpose.

3. Numerical procedures

a. Vertical differencing scheme

Discretization along the vertical is done by dividing the atmosphere into N equally spaced layers, each of a pressure thickness of $\Delta p = p_0/N$ [mb] as shown in Fig. 1. The numerical model equations are obtained by applying the vorticity equation at the midpoint of each layer and the omega equation at each level and approximating pressure derivatives by utilizing the centered finite differencing scheme. The values of $\bar{u}$, ϕ at the levels are assumed to be the average of their values at the adjacent upper and lower layers.

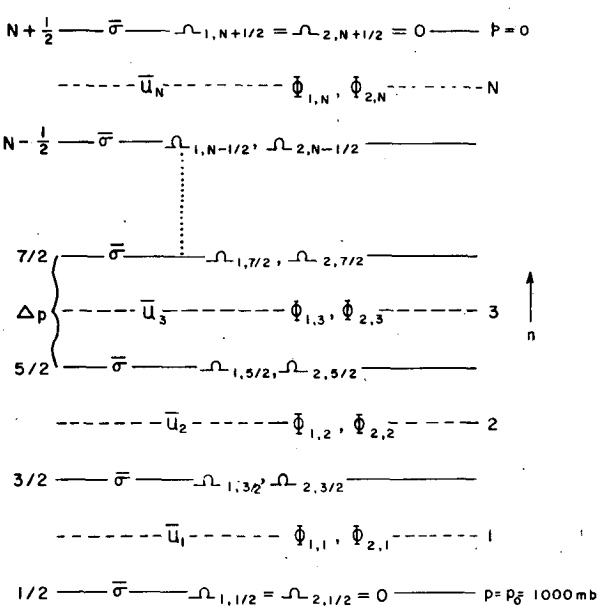

FIG. 1. Schematic diagram of the vertical level structure of the N-layer model

b. Spectral representation in meridional direction

In this study, the meridional distributions of the basic state zonal flow and perturbation are represented by truncated half-range cosine and sine Fourier series, respectively, as used by Mishra *et al.* (1981). The quasi-geostrophic spectral model based on the truncated Fourier series representation requires considerably less computer storage and time than a grid-point model. The spectral model is also free from the problem of nonlinear computational instability unlike grid-point models (Phillips, 1959).

The dependent variables are expressed as truncated sine Fourier series in y as

$$X(x, y, p, t) = \sum_{m=1}^{M} [X_{1m}(p, t) \cos kx + X_{2m}(p, t) \sin kx] \sin(mly), \quad (12)$$

where M is the order of truncation of the series, $l = \pi/D$ is the meridional wavenumber, k is the zonal wavenumber, X represents ω and ϕ and X_m are their spectral coefficients.

We express $\bar{u}(y, p)$ as

$$\bar{u}(y, p) = \sum_{j=0}^{J} u_j(p) \cos(jly), \quad (13)$$

where J is the order of truncation in the meridional wavenumber space and $u_j(p)$, $j = 0, 1, \ldots, J$, are the expansion coefficients, which are given by

$$\left.\begin{aligned} u_j &= \frac{2}{D}\int_0^D \bar{u}(y, p) \cos(jly)dy \\ u_0 &= \frac{1}{D}\int_0^D \bar{u}(y, p)dy \end{aligned}\right\}. \quad (14)$$

The spectral version of the vorticity and the omega equation is obtained by substituting Eqs. (12) and (13) for Eqs. (1) and (3), and are written in matrix form. The solution of the spectral omega equation is obtained by utilizing a matrix inversion method.

c. Time differencing scheme

In this study, the numerical solutions are obtained by time integration of the spectral model equations. For this purpose, the modified Euler backward time differencing scheme is used for the first time step and the leapfrog (centered) time differencing scheme is used for subsequent time steps. In order to damp the computational mode, the time filter suggested by Robert (1966) is used with a value of 0.01 for the filter parameter.

d. Initial wave perturbation

We describe a small initial wave perturbation as being confined to a single zonal wavenumber and hav-

ing no tilt in the vertical and meridional direction. In specifying the initial wave perturbation, care has been taken so that its amplitude maximum is close to the amplitude maximum of the unstable mode for the given zonal wavenumber. This will reduce considerably the number of days for which the model needs to be integrated before reaching the state of uniform exponential growth rate. For a meridionally symmetric jet, it is well-known that the most unstable mode structure along y has maximum amplitude at the center of a channel. This implies that the lowest spectral mode $m = 1$ dominates over the remaining modes with $m > 1$. We assume that initially at the vertical level n,

$$\phi_{2,m,n} = 0 \quad \text{for} \quad m = 1, 2, \ldots, M; \quad n = 1, 2, \ldots, N, \tag{15a}$$

and $\phi_{1,m,n}$ has an exponential distribution in m as

$$\phi_{1,m,n} = |\phi|_n e^{-m} \quad \text{for} \quad n = 1, 2, \ldots, N; \quad m = 1, 2, \ldots, M, \tag{15b}$$

where $|\phi|_n$ is the amplitude of the wave at the level n. Staley and Gall (1977) showed that the level of maximum wave amplitude depends on wavelength. Mishra and Salvekar (1980) have found a similar qualitative relation between the level of maximum wave amplitude and the wavelength for a mean monsoon zonal flow. We have prescribed a bell-shaped vertical profile for the wave amplitude, i.e.,

$$|\phi|_n = \phi_{\max}\alpha^2/[\{(n - \tfrac{1}{2})p - p_{\max}\}^2 + \alpha^2], \quad n = 1, 2, \ldots, N, \tag{16}$$

where α is the half-width of the wave amplitude profile, $p_{\max}$ the location of the profile maximum and $\phi_{\max}$ the maximum value of the wave amplitude; α (=100 mb) is kept constant for all the zonal wavelengths considered in this study. The location $p_{\max}$ is computed from the following relation for different wavelengths:

$$p_{\max} = \begin{cases} p_0 - 150(L-1), & \text{for} \quad 1 \leqslant L \leqslant 6 \\ 250\text{–}50(L-6), & \text{for} \quad 6 \leqslant L \leqslant 10 \\ 50 \text{ mb}, & \text{for} \quad L > 10 \end{cases}, \tag{17}$$

where L is the wavelength (10^3 km).

e. Growth rate and phase velocity

The vertical averaged growth rate and phase velocity spectra are computed at each time step by utilizing the formulas given by Brown (1969). The attainment of uniformity in the growth rate spectrum ν_m and the phase velocity spectrum c_m are indicative of the fact that the waves have reached a state of uniform exponential growth. For the termination of the model integration, we ensure that the growth rate spectrum is uniform within an accuracy of 10^{-3}.

4. Basic state parameters

The zonal wind distribution in a meridional plane and the vertical profile of basic stability are the two essential basic state parameters for performing the quasi-geostrophic, combined barotropic–baroclinic stability analysis.

a. Zonal wind

For obtaining the zonal wind distribution, the observed seasonal mean (June–August) winds at the standard pressure levels from the surface to 100 mb are subjectively interpolated on a 2.5° × 5° latitude–longitude grid in the region 4°S–32°N and 55°E–105°E from published charts of Newell *et al.* (1972). This choice of latitudinal width is motivated by the following considerations: 1) the width should be large enough to cover major meridional shear zones of the jet and 2) its midpoint should be close to the jet maximum. In choosing the longitudinal interval, the considerations kept in mind were that it should be comparable to the wavelength of the observed disturbances and that its midpoint should coincide with the jet maximum because most of the wave growth takes place around the jet maximum, as shown by Tupaz *et al.* (1978). The grid-point values are longitudinally averaged.

The observed meridional $\bar{u}$ profile at each standard isobaric level in the troposphere, *viz.*, 1000, 850, 600, 500, 300, 200, 150 and 100 mb, is fitted to a half-range cosine Fourier series. The first seven coefficients $u_0, u_1, \ldots, u_6$ at each pressure level are numerically computed. In order to avoid the generation of spurious small-scale fluctuations during the numerical computation of p derivatives of $\bar{u}$, the coefficients are represented analytically as a linear combination of the bell-shaped profiles (Mishra, 1980). The fitted profiles are presented in Fig. 2. The analytical zonal wind distribution in the meridional plane is computed from the fitted profiles of the Fourier coefficients shown in Fig. 3. A comparison between the observed wind and the analytic wind distributions indicates that the analytic representation is able to retain the main observed characteristics of the mean monsoon zonal wind distribution to a good degree of accuracy. A symmetric $\bar{u}(y, p)$ distribution was also obtained by neglecting the odd coefficients u_1, u_3, u_5 (not presented). The maximum difference between the asymmetric and symmetric $\bar{u}$ distributions was found to be less than 2 m s^{-1}. This does not rule out the possible significant contributions of the small antisymmetric components to the instability characteristics as shown by Mishra *et al.* (1981) for the barotropic case.

A comparison is also made between $\bar{u}$ profiles along the center of the channel at 14°N (as obtained from Fig. 3) and a profile used by Mishra and Salvekar (1980), which is obtained by averaging the wind over

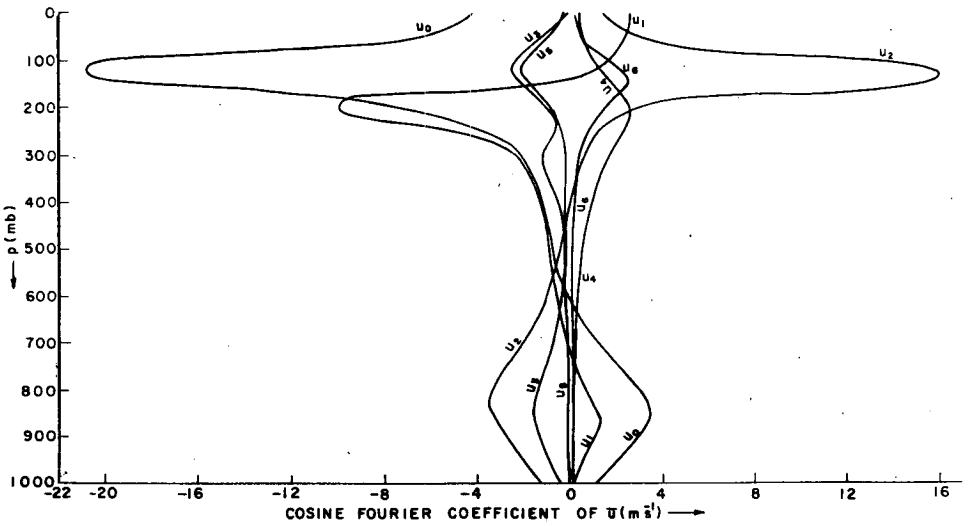

FIG. 2. Vertical profiles of the fitted cosine Fourier coefficients of the mean monsoon zonal wind.

a zonal distance of 2000 km. The two profiles are in very close agreement in the upper troposphere, while in the lower troposphere, the westerlies in the former are nearly half of the latter. This difference between the two profiles is due to the low level strong westerlies being confined in a longitudinal interval 65–85°E over the peninsular India, whereas the upper-tropospheric strong easterlies extend from the south China Sea to the eastern Atlantic Ocean.

b. Static stability

The computed mean inverse static stability ($1/\sigma$) profile, representative of the region of disturbances, is presented in Fig. 4. The observed $1/\sigma$ profile in the lower troposphere is more or less a straight line that decreases rather sharply with height in the upper troposphere. The observed inverse static stability profile is represented analytically as

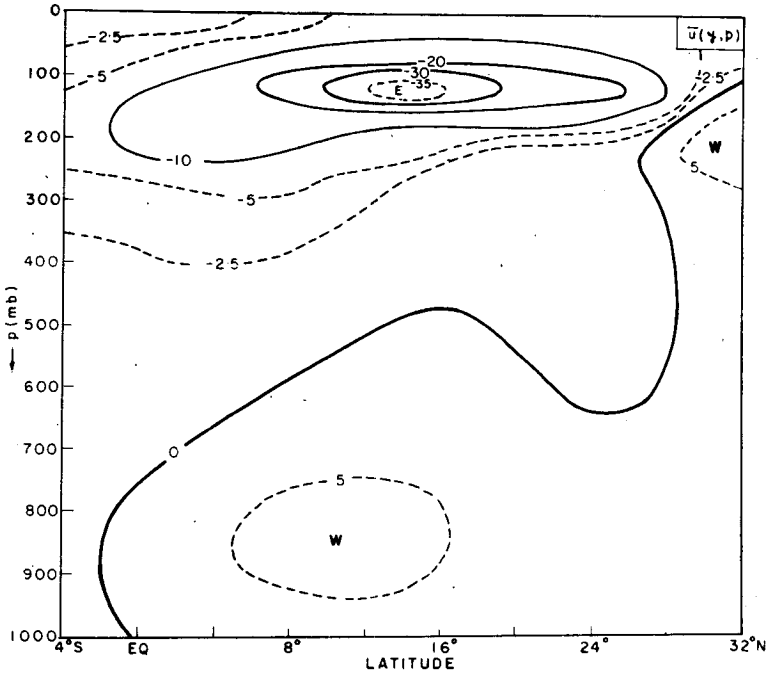

FIG. 3. Meridional plane distribution of fitted zonal wind.
Contour separation 10 m s^{-1}.

$$1/\sigma = \begin{cases} (5p/p_0 - 2)/(3\sigma_0) & \text{for } 600 \text{ mb} \leq p \leq p_0 \\ (5p/3p_0)^{1/2}/(3\sigma_0) & \text{for } 300 \text{ mb} \leq p \leq 600 \text{ mb} \\ (p/p_0)^2/(0.27\sqrt{2}\sigma_0) & \text{for } 0 \leq p \leq 300 \text{ mb} \end{cases}, \quad (18)$$

where σ_0 is the static stability at $p = p_0$ and has a value of 1/95. The analytic profile of $1/\sigma$ is also presented in Fig. 4, along with the observed profile. The figure shows that the analytical profile is close to the observed profile and is adequate for the present study.

c. Meridional distribution of $\bar{q}_y$

The latitude–height section of the computed $\bar{q}_y$ is shown in Fig. 5. It is seen from the figure that the necessary condition for barotropic–baroclinic instability is satisfied by the easterly jet at pressure levels close to its core, whereas the low-level westerly jet does not satisfy the necessary condition. A comparison between the distributions of $\bar{q}_y$ and $-\bar{u}_{yy}$ (not presented) indicated that the jet satisfies the necessary condition for baroclinic instability, in addition to the condition for barotropic instability. Further, the negative contributions by the baroclinic term $-(\bar{u}_p/\sigma)_p$ in the $\bar{q}_y$ field are much larger than the negative contributions by the barotropic term $-\bar{u}_{yy}$. A comparison of largest negative values of $\bar{q}_y$ for symmetric (not presented) and asymmetric wind profiles shows that the former is 40% less than the latter, which is quite significant.

5. Growth rate and phase speed spectra

The growth rate and zonal phase speed spectra for the asymmetric and the symmetric basic zonal wind distribution obtained from the numerical solution of the quasi-geostrophic model by using 20 layers in the vertical and a meridional spectral truncation $M = 8$ are presented in Figs. 6a and 6b, respectively. This spectral truncation was found to be adequate after comparing the solutions with different meridional truncations. For obtaining the numerical solutions, zonal wavelengths in the range of 1000–10 000 km at intervals of 500 km are considered. The waves in the short-wavelength region (1000 km $\leq L \leq$ 2500 km) are found to be stable. It is known that the growth of short waves is controlled by the wind shears in the lower troposphere (Mishra and Salvekar, 1980). It can be seen from Fig. 5 that the necessary condition for instability is not satisfied in the lower troposphere. The growth rate spectra are seen to have a sufficiently sharp peak. The preferred barotropic–baroclinic unstable wavelengths for the symmetric and asymmetric easterly

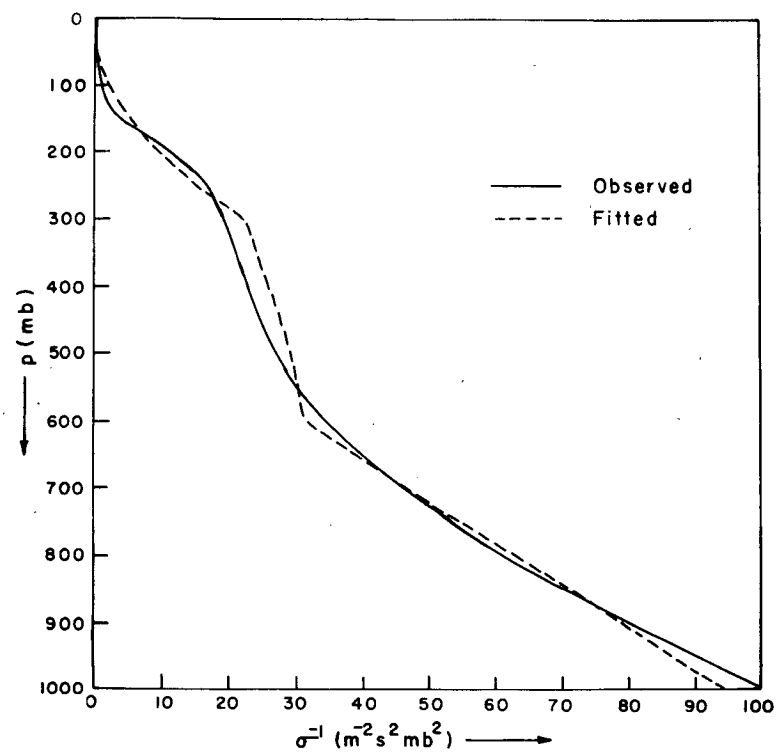

FIG. 4. Vertical profile of the mean observed inverse static stability averaged over the area 55–105°E and 0–20°N for the summer monsoon and the fitted profile.

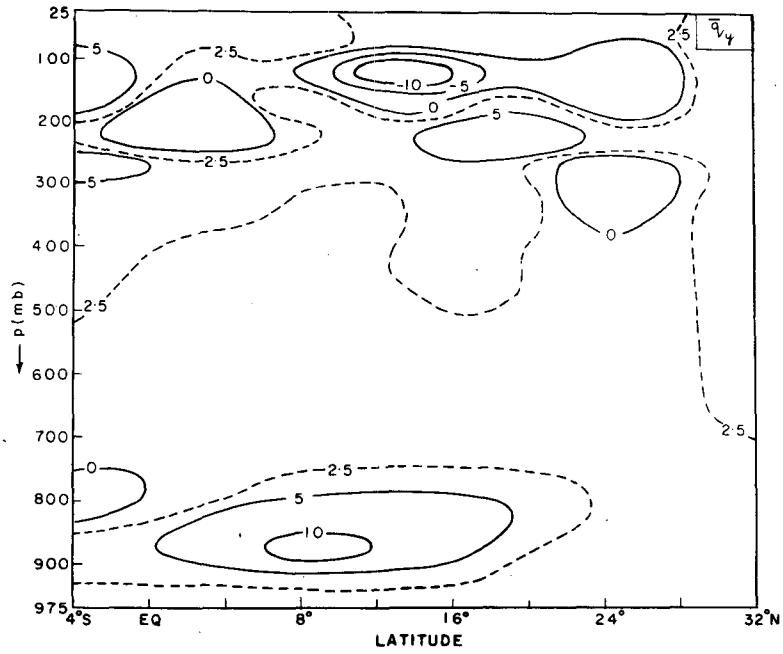

FIG. 5. Meridional plane distribution of potential vorticity gradient ($\bar{q}_y$) for the asymmetric zonal wind distribution. Contour separation 5×10^{-11} m^{-1} s^{-1}.

jets are nearly the same and are equal to 6500 km as obtained from the growth rate spectra. The preferred phase speeds are -17.8 and -20.5 m s^{-1} and the growth rates are 0.32 and 0.34 day^{-1} for the symmetric and asymmetric jets, respectively.

The growth rate and phase speed spectra were also obtained in the presence of Ekman boundary-layer friction (not presented) for the symmetric and asymmetric cases. It was found that the friction does not have any significant effect on the growth rates and phase speeds for wavelengths of more than 4000 km. Further, the maximum growth rate obtained from the 10-layer model is ~25% less than the value for the 20-layer model.

The preferred wavelength and phase speed for the combined case are slightly less than the corresponding values for the barotropic case (Mishra *et al.*, 1981), but the growth rate for the combined case is significantly larger than for the barotropic case. This indicates that the baroclinic contribution to the combined growth rate is, in any case, not less than the barotropic contribution. The period associated with the asymmetric wave is 3.8 days. This value is very close to a preferred time period as found by Krishnamurti and Bhalme (1976) from a spectral analysis of the easterly jet at 200 mb.

The link between the linear dynamic instability theory and the observed disturbances is provided by the basic assumption that the theoretical wave with the highest growth rate would be the one most likely to be observed in the atmosphere. Furthermore, based on this assumption, it is expected that the observed peak in the transient kinetic energy spectrum corresponds to the wavelength of maximum linear growth rate. This is equivalent to saying that the most unstable wave would attain the largest amplitude. It has been suggested by some recent studies (Gall, 1976; Blakeslee and Gall, 1978) that a large difference between the preferred wavenumbers inferred from the transient kinetic energy spectrum of nonlinear experiments and the linear growth rate spectrum may be due to the presence of strong nonlinear energy exchanges between wavenumbers and nonlinear friction in the experiments. They found that this is particularly true for the fairly flat growth rate spectrum. If the growth rate spectrum is sufficiently peaked, as found in this study, the maximum energy is still found in the wavelength of maximum growth rate.

6. Computed structure of the preferred wave

In this section, we present the normalized structure of the most unstable asymmetric wave of wavelength 6500 km. Krishnamurti (1971) found that the upper tropospheric transient wave at 200 mb during the northern summer of 1967 has an average maximum meridional wind speed of 4 m s^{-1}. Taking into consideration that the wave amplitude at 200 mb is nearly half of the maximum value at 125 mb, we prescribe a maximum meridional wind amplitude of 8 m s^{-1} for computing the structure and energetics of the preferred wave.

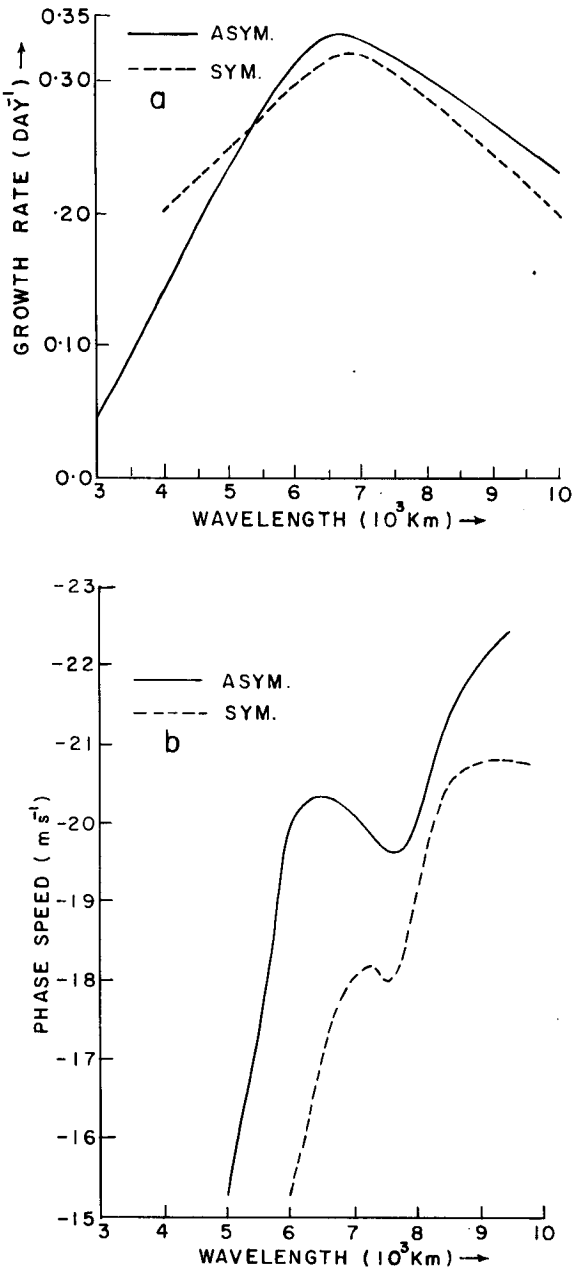

FIG. 6. (a) Growth rate spectrum and (b) phase speed spectrum of symmetric (dashed line) and asymmetric (solid line) waves.

a. Geopotential field

The meridional plane distributions of the geopotential wave amplitude and phase of the preferred wave are presented in Figs. 7a and 7b, respectively. The geopotential amplitude maximum is located at the center of the channel. In a barotropic asymmetric case, a maximum geopotential wave amplitude has been found to be located to the south of the easterly jet center by Mishra *et al.* (1981). Whereas, in a pure baroclinic case the most unstable mode has a geopotential maximum at the center of the channel (Mishra and Salvekar, 1980), similar to the combined case presented here. From the above discussion, it can be concluded that the baroclinic process dominates over the barotropic process in the combined model. However, the close resemblance between the observations and the barotropic unstable wave suggests that in nature, barotropic processes are not less important than the baroclinic processes. We feel that in the combined case also, the wave amplitude maximum will move closer to the equator provided that the jet's sloping nature in the meridional plane is properly resolved in the model.

The wave has a significant tilt with height and latitude in the upper troposphere. The vertical tilt with height is eastward below the jet level and westward above the jet level. Furthermore, the vertical tilt is rather sharp around the jet level and it is opposite to the vertical shear of the basic zonal current. This situation is favorable for the growth of the wave due to the baroclinic instability mechanism. The pronounced horizontal tilt is found in the 75–175 mb layer. The horizontal tilt is eastward with latitude throughout the channel at 125 mb, which implies southward transport of easterly momentum in the channel. At 175 mb, the horizontal tilt with latitude is eastward to the south and westward to the north of the jet center. This indicates that the growth of the wave is, to some extent, due to the barotropic energy conversion at these levels.

b. Vertical velocity field

The maximum vertical velocity is found at 150 mb and just to the north of the jet center as seen from the omega amplitude distribution (Fig. 8a). A comparison between the geopotential and vertical velocity phases (Figs. 7b and 8b) indicates that below the jet level, the maximum upward motion at each level is to the west of the geopotential wave trough at a distance less than $L/4$, while above the jet level, the maximum upward motion is located to the east of the trough. It may be relevant to mention that in baroclinic unstable modes of midlatitude westerly zonal currents, a maximum upward motion lies to the east of the wave trough at a distance of $L/4$ (Charney, 1947; Kuo, 1952). The relative configuration between the geopotential and omega wave indicates a downward (upward) transport of the wave kinetic energy below (above) the jet level. The horizontal and vertical phase tilts of the omega wave are similar to the tilts of the geopotential wave.

c. Temperature field

The maximum perturbation temperature is 2.2°C (Fig. 9a). It can be concluded from Figs. 8b and 9b that in the 75–225 mb layer, the warm air is rising to the west of the wave trough and the cold air is sinking to the east of the trough in the latitudinal belt 8–24°N.

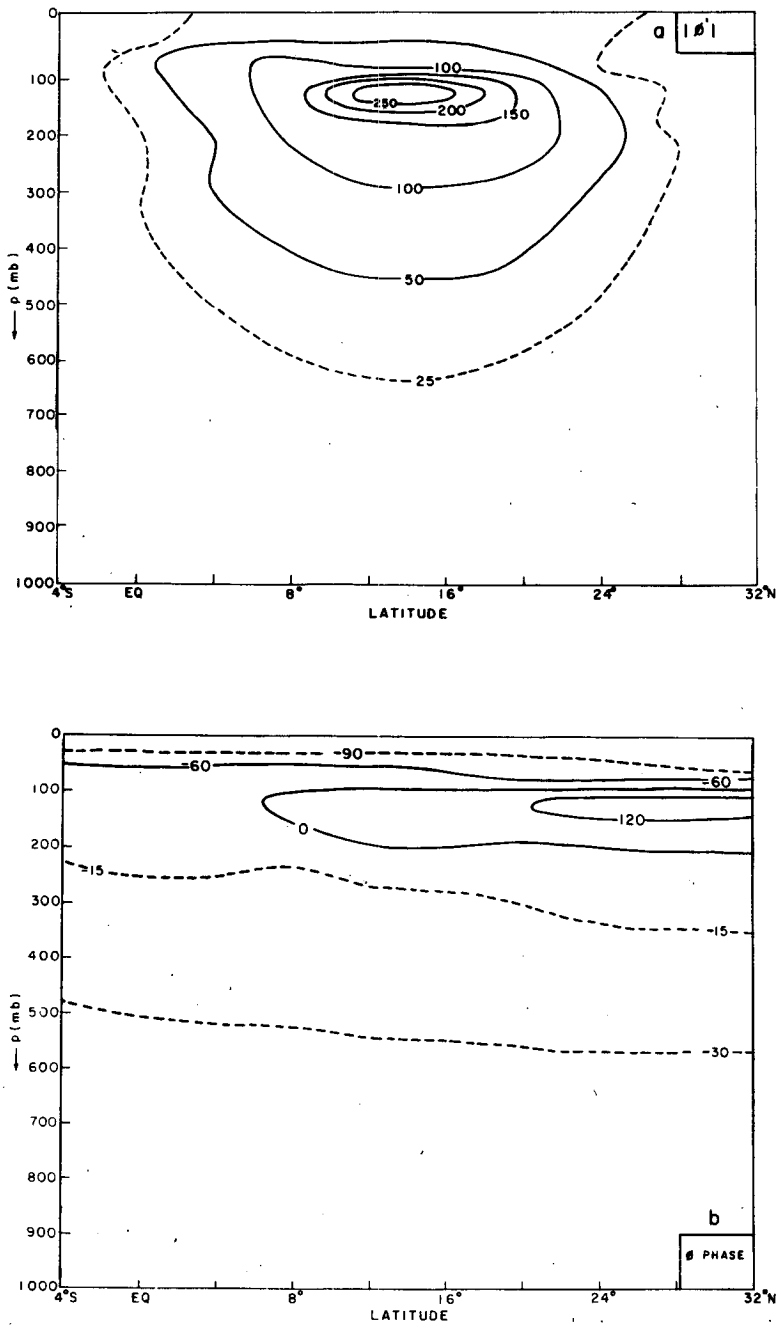

FIG. 7. Meridional plane distribution of the asymmetric preferred geopotential wave ϕ': (a) amplitude (contour separation 50 m^2 s^{-2}) and (b) phase (contour separation 60°).

This process will lead to the conversion of wave available potential energy into wave kinetic energy. Thus, the baroclinic energy source for the growth of waves lies in the 75–225 mb layer. Furthermore, in the lower troposphere, the phase difference between the omega and temperature waves is nearly 90°, which indicates that the conversion between P_w and K_w is very small.

d. Vertical scale

The vertical scale of the preferred wave is defined as the latitudinally-averaged vertical half-width of the geopotential wave amplitude. The half-width at different latitudes is computed from the geopotential wave amplitude distribution presented in Fig. 7a. The vertical

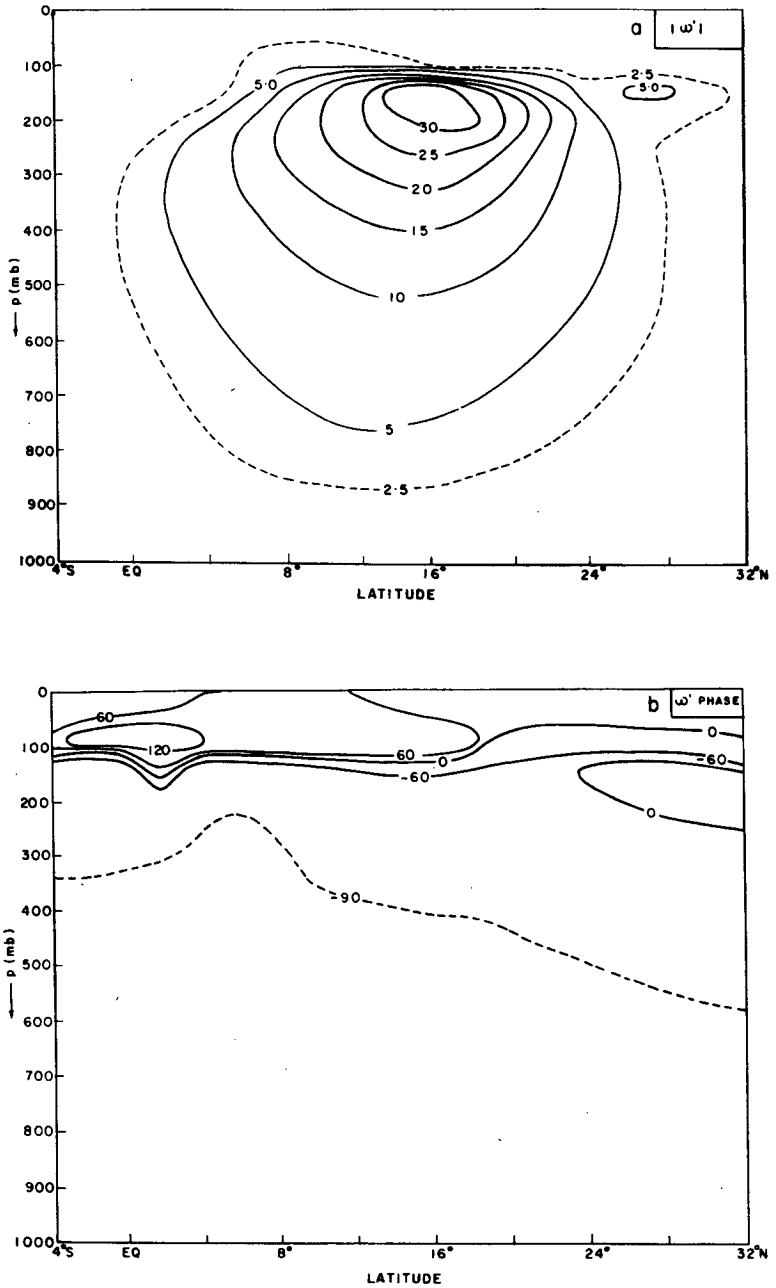

FIG. 8. (a) As in Fig. 7(a) with contour separation 5×10^{-5} mb s^{-1} except for vertical velocity ω' and (b) as in Fig. 7(b).

half-width at the center of the channel (14°N) is smallest with a value of 75 mb; away from the center the value increases, reaching 300 and 250 mb at 8 and 20°N, respectively. The average value of the vertical half-width in the latitudinal belt 8–20°N is found to be 125 mb, which is close to the vertical scale of the mean monsoon current (Mishra and Salvekar, 1980). Thus, the vertical scale of the preferred wave is equal to the vertical scale of the basic zonal wind.

e. Meridional scale

The meridional scale of the easterly jet varies in the vertical. The computed vertical average meridional scale of the jet in the 75–225 mb layer is about 2700 km, which is comparable to the value at 100 mb. The averaged meridional half-width of the preferred wave in the 75–225 mb layer is 1650 km as obtained from the geopotential wave amplitude distribution. The me-

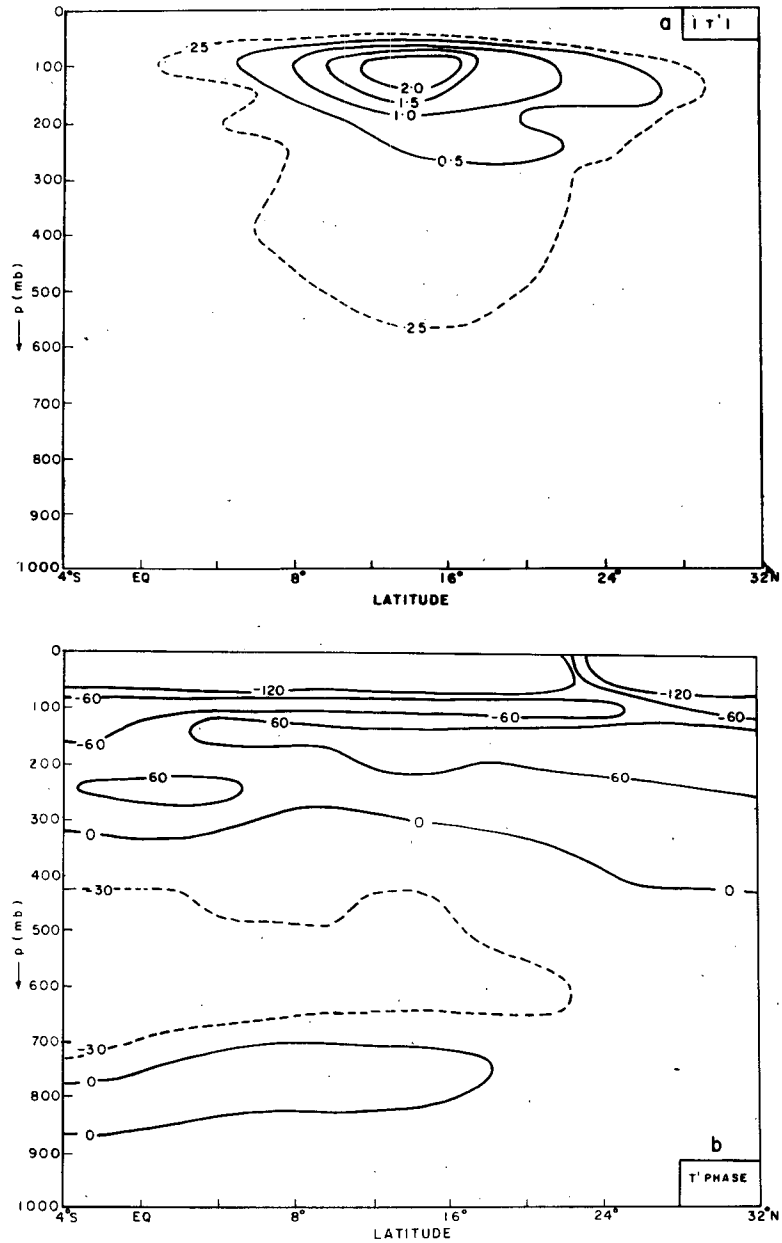

FIG. 9. (a) As in Fig. 7(a) with contour separation 0.5°C except for temperature wave T' and (b) as in Fig. 7(b).

ridional scale for the combined case is in good agreement with the value obtained for a barotropic preferred wave in the monsoon easterly jet (Mishra *et al.* 1981). The computed average radius of curvature of the easterly jet with respect to latitude at the center $[=(\bar{u}/\bar{u}_{yy})^{1/2}]$ in the 75–225 mb layer is ~750 km. Finally, we conclude that the meridional scale of the barotropic–baroclinic wave is nearly equal to the geometric mean of the radius of curvature and the meridional scale of the easterly jet. A similar result has been found for the barotropic case by Mishra *et al.* (1981).

f. Zonal scale

We have chosen $2k^{-1}$ as the zonal scale. This scale is also close to the half-width around a maximum of the wave field distribution in the zonal direction. By using this definition, the zonal scale of the preferred wave is obtained as 2135 km. The Rossby radius of deformation for the tropical upper troposphere is ~2000 km as has been mentioned earlier in Section 2a. Thus, the zonal scale of the preferred wave is close to the Rossby radius of deformation.

7. Meridional transports

a. Zonal momentum

It can be seen from Fig. 10, where the distribution of meridional transport of zonal momentum by the preferred wave in the meridional plane is presented, that at most of the latitudes in the upper troposphere, the easterly momentum transports are southward with a maximum value of 15 $m^2 s^{-2}$ located ~10°N at 125 mb. Furthermore, the momentum transports are mostly concentrated in a narrow vertical layer around the jet level. The computed momentum transports are qualitatively in gross agreement with the observed transient eddy momentum transports (Newell *et al.* 1972). In the case of the symmetric wave, the easterly momentum transports are southward to the south of the jet center and northward to the north of the center with a maximum value of 3 $m^2 s^{-2}$ close to the center (not presented). From the above results, we conclude that the antisymmetric components of the jet are mainly responsible for the observed momentum transports in the vicinity of the easterly jet. A similar conclusion was arrived at for the barotropic case (Mishra *et al.*, 1981). Furthermore, the significant barotropic energy conversion from the basic state kinetic energy to the wave kinetic energy can occur in the narrow vertical layer.

b. Sensible heat

The significant southward sensible heat transports by the unstable wave are found in the upper troposphere and particularly in the 150–200 mb layer (Fig. 11). Above this layer the transports are northward. The average observed southward sensible heat transport by the transient eddies in the longitudinal interval 55–105°E is ~2.5 m s^{-1} °C (Newell *et al.*, 1974), which is in agreement with the computed heat transport in this study. The heat transports below and above the jet level are down the basic state meridional temperature gradient. This process will lead to the conversion of the basic state available potential energy into the wave available potential energy.

8. Computed energetics of the preferred wave

The computed vertical profiles of the wave energies $\{K_w\}$ and $\{P_w\}$, the energy conversions $C\{K_b, K_w\}$, $C\{P_w, K_w\}$ and the convergence of wave energy flux VK_wC are presented in Fig. 12. A positive value of VK_wC indicates the wave kinetic energy convergence in the vertical layer and a negative value indicates the divergence of the wave kinetic energy from the layer. The vertical distribution of the wave energies indicates that the combined unstable wave is characterized by a shallow wave. This is due to the presence of significant vertical and meridional shears of the basic zonal wind in the narrow vertical layer around the jet level and the large static stability above the jet level.

It is seen from the energy conversion profiles that the maximum positive conversion $\{P_b, P_w\}$ is about four times that of the maximum positive barotropic energy conversion $\{K_b, K_w\}$. Also, the baroclinic energy conversion occurs in a vertical layer of thickness greater than the layer of the positive barotropic energy conversion. These results suggest that the baroclinic in-

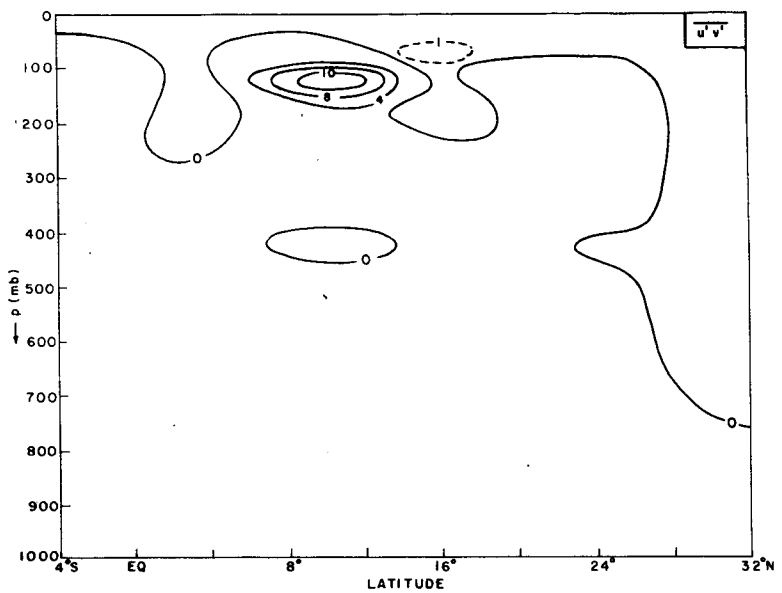

FIG. 10. Meridional plane distribution of zonal momentum transport $\overline{u'v'}$ by the asymmetric preferred wave. Contour separation 4 $m^2 s^{-2}$.

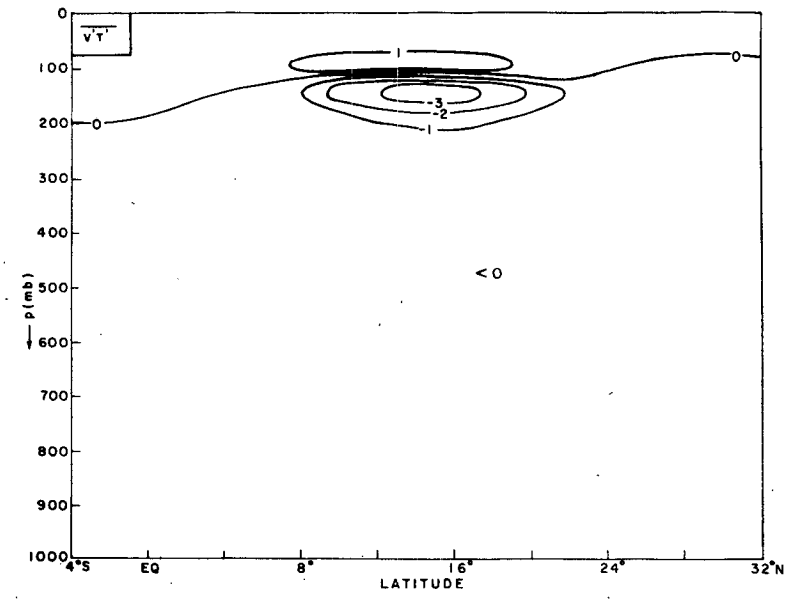

FIG. 11. As in Fig. 10 except for sensible heat transport $\overline{v'T'}$. Contour separation 1 m s^{-1} °C.

stability dominates over the barotropic instability in wave growth. The wave receives the kinetic energy from the basic state kinetic and available potential energies around the jet level and away from it, the wave gains the kinetic energy through the process of vertical wave kinetic energy flux convergence.

The vertically integrated wave energies and the wave energy conversions are shown in Fig. 13. From the figure, it can be concluded that the unstable wave receives the kinetic energy from both P_W and K_B with much larger contribution from the former than the latter.

9. Zonal propagation of unstable waves

The unstable waves propagate westward with a phase speed less than the maximum easterly jet speed. The waves propagate in the direction of basic zonal flow. From this fact, one may conclude that the advection of vorticity is mainly responsible for their westward propagation. However, the wave phase speed does not vary with height, whereas the advection does vary with height. This indicates that other physical processes, namely the Laplacian of thermal advection, the differential vorticity advection and the beta effect, would

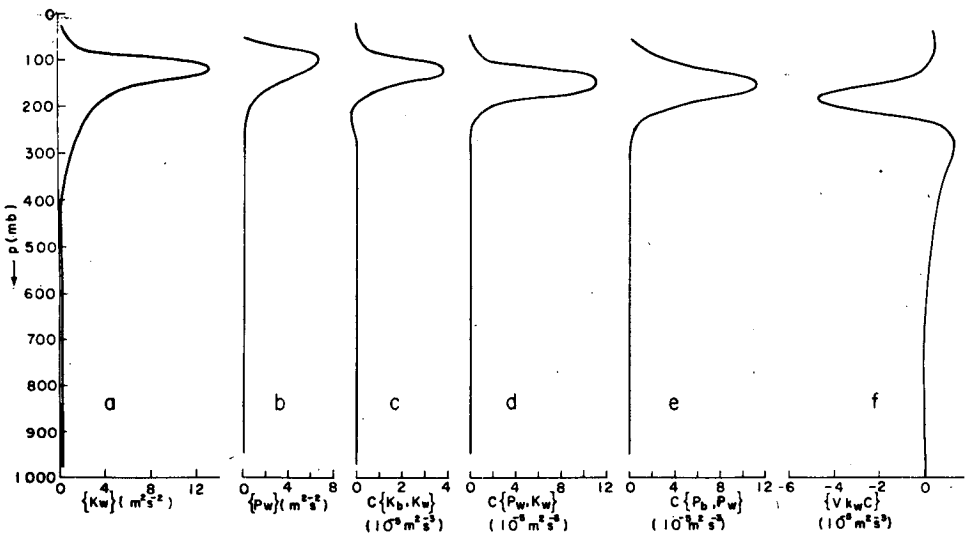

FIG. 12. Vertical profiles of horizontally averaged wave energies and energy conversions and convergence of wave energy flux for the asymmetric preferred wave.

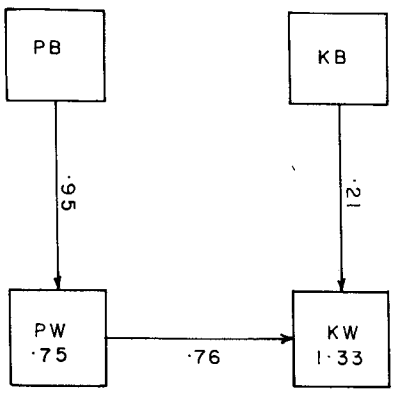

FIG. 13. Flow diagram of energy integrated over the mass of the entire vertical column of the unit horizontal area, the energy flow being in the direction of the arrow. Energies P_w and K_w are in units of J m^{-2} and energy conversions are in units of 10^{-5} J m^{-2} s^{-1}.

maintain the uniformity in the phase speed. In this section, we propose to quantify the contributions of the various physical processes in the westward propagation of the waves.

The zonal wave phase speed (c_r) of the exponential growing wave, which is independent of y and p, can be written as

$$c_r = c^{\xi}(y, p) + c^{\beta}(y, p) + c^{T}(y, p) + c^{\zeta}(y, p), \quad (19)$$

where c^{ξ}, c^{β}, c^{T} and c^{ζ} denote the phase velocity due to the relative vorticity advection, the beta effect, the Laplacian of thermal advection and the differential vorticity advection, respectively. The phase speed due to the individual physical processes is a function of y and p.

According to Brown (1969), c_r in terms of the wave components ϕ_1 and ϕ_2 is given by

$$c_r = k^{-1}(\phi_1\phi_{2,t} - \phi_2\phi_{1,t})/(\phi_1^2 + \phi_2^2). \quad (20)$$

The Laplacian of thermal advection and the differential vorticity advection contribute to the geopotential tendency through their induced divergence field. If the divergence and geopotential waves are in phase or in opposite phase, the divergence effect will not influence phase propagation. The most favorable situation for westward wave propagation due to the divergence effect occurs when the phase difference between the divergence and geopotential wave fields is $\pi/2$ with the convergence located to the west of the geopotential wave trough. Convergence to the west of trough will generate cyclonic vorticity in the west, whereas divergence to the east of the trough will generate anticyclonic vorticity in the east. This will contribute to the movement of the geopotential wave in the westward direction.

The geopotential tendency due to each physical process is computed for the asymmetric preferred wave at each vertical level, and at intervals of 2° latitude. The tendency ω' due to the Laplacian of thermal advection and differential vorticity advection is computed from the omega equation. The computed vertical profiles of latitudinally averaged c^{ξ}, c^{β}, c^{T} and c^{ζ}, as computed from Eq. (20), are presented in Fig. 14. The steering level (at which $c = c_r$) is located at 150 mb.

It can immediately be seen from the profiles that the westward propagation of the wave due to the horizontal advection of relative vorticity exceeds the wave phase speed only in the 150–100 mb layer, and away from this layer the speed decreases rather sharply. Furthermore, in the 150–100 mb layer, the eastward propagation due to the differential vorticity advection nearly balances the westward propagation due to the horizontal advection. The wave motion due to the Laplacian of thermal advection is rather small and westward throughout the atmosphere except for the 125–25 mb layer, where it is relatively large. The contribution of the Laplacian of thermal advection to the westward movement of the wave is smaller than that of the other physical processes. It can be concluded from the figure that the beta effect contributes nearly uniform westward motion to the wave throughout the atmosphere with an average value of 15 m s^{-1}, which is quite close to the phase speed of the preferred wave. Also, for $\beta = 0$, the westward phase speed was found to be only 4 m s^{-1}.

10. Conclusions

We have determined the combined barotropic–baroclinic instability characteristics of the upper tro-

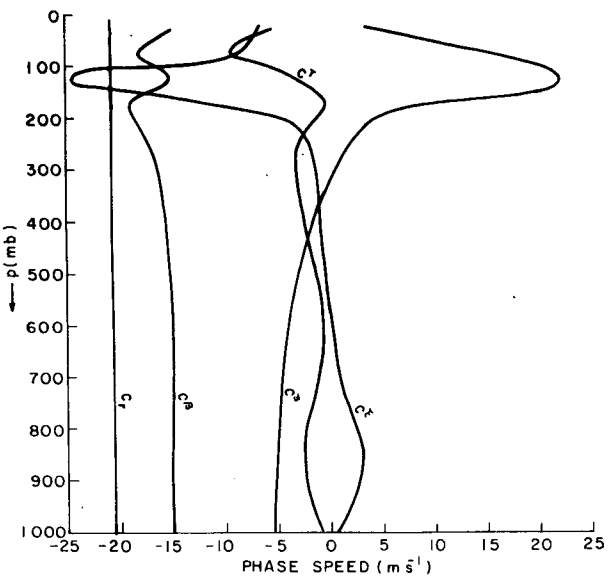

FIG. 14. Vertical profiles of zonal phase speed due to relative vorticity advection c^{ξ}, beta effect c^{β}, Laplacian of thermal advection c^{T}, differential absolute vorticity advection c^{ζ}, and the total phase speed c_r, all in units of m s^{-1}.

pospheric tropical easterly jet. We have concluded from the growth rate spectrum that the observed disturbances in the vicinity of the jet are likely to be excited by the combined barotropic–baroclinic instability mechanism. It has been found that the antisymmetric part of the easterly jet causes a significant increase in the growth rates for wavelengths larger than the preferred wavelength, but for wavelengths smaller than the preferred wavelength, it causes a decrease in the growth rates.

The computed structure of the preferred wave has indicated that its meridional scale is determined by the meridional shear of the zonal wind and its vertical scale is related to the vertical scale of the basic zonal wind profile. The wave zonal scale has been found to be equal to the Rossby radius of deformation.

It has been found that large equatorward transports of easterly momentum are mainly due to the presence of antisymmetric components in the easterly jet. The computed momentum and sensible heat transports are found to be in gross agreement with the observed transports by eddies.

It has been shown that the energy source for the unstable wave is located in a narrow vertical layer around the jet level. Away from this layer, the energy for the wave growth is provided by the convergence of wave kinetic energy flux. During the initial wave growth, the baroclinic energy conversion dominates over the barotropic energy conversion.

In the upper troposphere, the westward phase speed due to the horizontal advection of relative vorticity is nearly balanced by the eastward phase speed due to the differential vorticity advection. The contribution of the Laplacian of the thermal advection process is generally small throughout the troposphere. It has been concluded from the results that the beta effect is mainly responsible for the westward movement of the wave.

It seems that the barotropic features (momentum transports and meridional scale) of the combined unstable mode are very close to the pure barotropic mode and that its baroclinic features (heat transports and vertical scale) are very close to the pure baroclinic mode. This may be due to the fact that both pure barotropic and pure baroclinic modes have nearly equal preferred wavelengths and their energy sources are located in nearly the same vertical layer. The common feature of two modes, *viz.*, location of amplitude maxima, is determined by the baroclinic mode because the baroclinic instability is much stronger than the barotropic instability in the model.

This study seems to provide a possible qualitative basis for an explanation of the existence and maintenance of the upper tropospheric disturbances along the easterly jet. There are many observed features of the disturbances which are missing from the unstable modes. The observed momentum transports due to eddies across the easterly jet center are quite large, while the momentum transports by the asymmetric unstable wave are quite small compared to the values away from the center. A stability analysis of the jet over a sphere is likely to account for the observed momentum transports as indicated by various recent studies for midlatitude flows.

A study in the nonlinear regime may bring the unstable modes still closer to reality because the observed characteristics of the disturbances are, to a large extent, representative of finite amplitude disturbances where the nonlinear effects are not insignificant.

Acknowledgments. We are grateful to Dr. R. Ananthakrishnan for his scientific comments on various aspects of this study and to Dr. Bh. V. Ramana Murty, Director, for his keen interest in this study. The authors would like to thank one of the anonymous reviewers for very useful suggestions, which led to a significant improvement in the presentation of the paper. Thanks go to Smt. V. V. Savant for typing the manuscript.

REFERENCES

Blakeslee, R., and R. Gall, 1978: The effect of meridional circulation on the baroclinic instability of the winter zonal flow. *J. Atmos. Sci.*, **35**, 2368–2372.

Brown, J. A., 1969: A numerical investigation of hydrodynamic instability and energy conversions in the quasi-geostrophic atmosphere. Part I. *J. Atmos. Sci.*, **26**, 352–365.

Charney, J. G., 1947: The dynamics of longwaves in a baroclinic westerly current. *J. Meteor.*, **4**, 135–163.

Colton, D. E., 1973: Barotropic scale interaction in the tropical troposphere during the northern summer. *J. Atmos. Sci.*, **30**, 1287–1302.

Estoque, M. A., and M. S. Lin, 1977: Energetics of easterly waves. *Mon. Wea. Rev.*, **105**, 582–589.

Gall, R., 1976: A comparison of linear baroclinic instability theory with the eddy statistics of a general circulation model. *J. Atmos. Sci.*, **33**, 349–373.

Krishnamurti, T. N., 1971: Observational study of the tropical upper tropospheric motion field during the Northern Hemisphere summer. *J. Appl. Meteor.*, **10**, 1066–1096.

——, and H. N. Bhalme, 1976: Oscillation of a monsoon system: Part I. Observational aspects. *J. Atmos. Sci.*, **33**, 1937–1954.

Kuo, H. L., 1952: Three-dimensional disturbances in a baroclinic zonal current. *J. Meteor.*, **9**, 260–278.

Mak, M. K., 1975: The monsoonal mid-tropospheric cyclogenesis. *J. Atmos. Sci.*, **32**, 2246–2253.

——, and C.-Y. J. Kao, 1979: An instability study of the onset-vortex of the southwest monsoon, 1979. *Tellus*, **34**, 358–368.

Mishra, S. K., 1980: Some analytical vertical profiles of monsoonal zonal wind over India. *Arch. Meteor. Geophys. Bioklim.*, **A29**, 109–117.

——, and P. S. Salvekar, 1980: Role of baroclinic instability in the development of monsoon disturbances. *J. Atmos. Sci.*, **37**, 383–394.

——, D. Subrahmanyam and M. K. Tandon, 1981: Divergent barotropic instability of the tropical asymmetric easterly jet. *J. Atmos. Sci.*, **38**, 2164–2171.

Mokashi, R. Y., 1974: The axis of the tropical easterly jet stream over India and Ceylon. *Indian J. Meteor. Hydrol. Geophys.*, **25**, 55–68.

Newell, R. E., J. W. Kidson, D. G. Vincent and G. J. Boer, 1972 and 1974: *The General Circulation of the Tropical Atmosphere and Interactions with Extratropical Latitudes.* Vols. 1 and 2. The MIT Press, 258 pp. and 370 pp.

Phillips, N. A., 1954: Energy transformations and meridional circulation associated with simple baroclinic waves in a two-level, quasi-geostrophic model. *Tellus*, **6**, 273–286.

——, 1959: An example of nonlinear computational instability. *The Atmosphere and the Sea in Motion.* The Rockefeller Institute Press, 501–504.

Robert, A. J., 1966: The integration of low order spectral form of the primitive meteorological equations. *J. Meteor. Soc. Japan*, **44**, 237–245.

Salvekar, P. S., and S. K. Mishra, 1984: Energetics and vertical structure of the baroclinic modes of the monsoonal zonal flow. Submitted to *J. Atmos. Sci.*

Shukla, J., 1977: Barotropic–baroclinic instability of mean zonal wind during summer monsoon. *Pure Appl. Geophys.*, **115**, 1449–1462.

Staley, D. O., and R. L. Gall, 1977: On the wavelength of maximum baroclinic instability. *J. Atmos. Sci.*, **34**, 1679–1688.

Tupaz, J. B., R. T. Williams and C.-P. Chang, 1978: A numerical study of barotropic instability in a zonally varying easterly jet. *J. Atmos. Sci.*, **35**, 1265–1288.